Mineralogy and Shock Effects in Martian Breccia Northwest Africa 7034 by *In Situ* Micro X-ray Diffraction.

F. Cao[1], R. L. Flemming[1], M. R. M. Izawa[1,2], C. B. Agee[3], [1]Dept. Earth Sciences & Institute for Earth and Space Exploration, Western University, London, Ontario, Canada N6A 5B7 (fcao23@uwo.ca). [2]Institute for Planetary Materials, Okayama University, Misasa, Tottori, 682-0193, Japan. [3]C. B. Agee, Institute of Meteoritics, University of New Mexico, Albuquerque, 87131, USA.

Introduction: Nicknamed "Black Beauty" Northwest Africa (NWA) 7034 represents Martian regolith and is classified as a basaltic breccia [1]. "Black Beauty" contains multiple lithologies in a basaltic matrix (e.g., Fig. 1) and chemically resembles outcrops sampled by Spirit and Curiosity rovers [1-3]. Martian breccia meteorites have complex histories, including pre-launch shock events and brecciation, sedimentation as an impact breccia, thermal annealing and alteration on the Martian surface, launch-related impact effects, and terrestrial alteration [4–6]. Nevertheless, there are limited quantitative studies about the shock effects of mineral and lithic fragments in Martian breccias. The impact history recorded in these fragments is still not fully understood.

Optical petrography is a well-established method of assessing shock effects through observing the shock-induced microscopic deformation and textural features under the polarizing microscope [7-9], but has important limitations. These include the requirement of numerous reasonably large optically transmissive mineral grains, and the fact that quantitatively relating optical phenomena to previous shock conditions is difficult, and calibrations are limited to relatively few mineral species. *In situ* micro X-ray diffraction (μXRD) provides a quantitative approach to assessing shock metamorphism of shocked minerals in meteorites, such as olivine [10,11], pyroxene [12], and plagioclase [13] through measuring the degrees of progressive elongation of diffraction spots (or streakiness) along the Debye rings – here defined by the angular parameter chi (χ) direction and quantified as the full width at a half maximum along χ (FWHMχ) as well as diffraction line broadness in 2θ direction [14]. Previous studies imply feldspars and pyroxenes are the two most abundant crystal clasts in Martian breccias [1]. Here we focus on these two minerals to examine the shock effects using μXRD.

Micro-XRD not only determines mineral phases in Martian breccias but also yields information about grain size. Fine-grained minerals (< 5 μm) such as plagioclase and pyroxene in the matrix of Martian breccias, polycrystalline clasts, or secondary reaction products yield homogeneous Debye rings, while very fine-grained or nanocrystalline minerals (< 0.2 μm), such as magnetite and maghemite, can be identified by broadening in 2θ [15,16]. In addition, the grain size of coarse-grained materials (> 15 μm) can also be quantified by the radial integration of the Debye rings by counting the number of spots [17,18].

The goals and objectives are: (a) Identify mineral variations between the matrix and clasts in Martian breccias; (b) Characterize mineral textures such as grain size and crystallinity; (c) Determine the shock level experienced by plagioclase and pyroxene.

Sample and Methodology: Micro-XRD was performed using a Bruker-AXS D8 Discover μXRD with a 300 μm nominal beam diameter, using CoKα radiation (λ = 1.7889 Å) (operating at 35 kV and 45 mA), a Vantec-500 Area Detector with General Area Detector Diffraction System (GADDS) software. Two-dimensional (2D) XRD images were integrated to produce either intensity vs. 2θ plots over the 2θ range from 24° to 100°, with step size 0.024°, or intensity vs. χ plots. Minerals were identified using the International Center for Diffraction Data (ICDD) database. Strain-related mosaicity or misorientation of sub-grains that causes peak broadening along the Debye rings or chi (χ) direction was studied. A single unshocked crystal produces one or more diffraction spots, each of which represents a family of lattice planes defined by a Miller index (hkl). Plastically deformed crystals, caused by the impacts, show discontinuous streaking characteristics along the Deybe rings in their 2D XRD images. FWHMχ along the chi dimension was measured using WIRE with peak fitting. More detailed information about the apparatus and μXRD technique is available in [12,19].

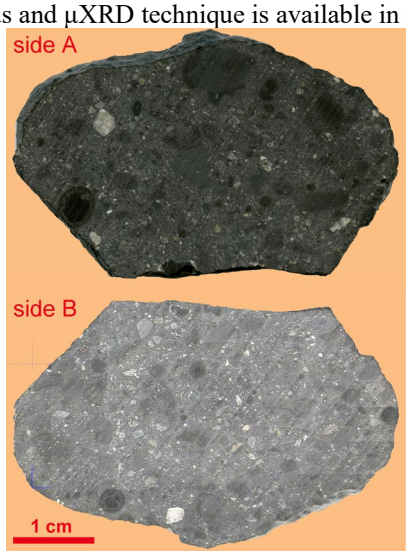

Fig. 1. Unpolished slab of NWA 7034 in this study (side A & B).

Results: *Mineralogy and grain size: Micro-XRD* investigation of various clasts and matrix show lithic clasts on both sides to contain coarse- to fine-grained mixtures of orthopyroxene (opx), clinopyroxene (cpx), plagioclase, and magnetite, as well as occasional apatite, pyrite, hematite, and ilmenite. Olivine is found in two separate spherules (A-13 and B-42). The olivine from spherule B-42 shows slightly streaked diffraction spots, while olivine from spherule A-13 shows extensively streaked diffraction spots. In this case, streaking is likely a textural effect of rapid growth.

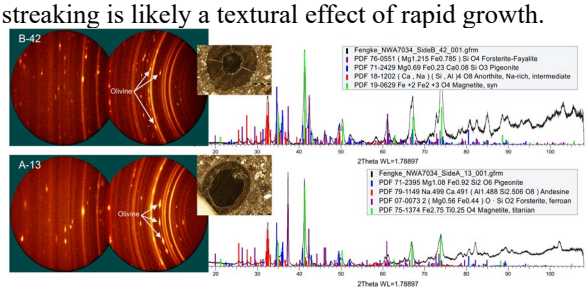

Fig. 2. Photographs of two spherules in NWA 7034 with 2D XRD images and their XRD patterns showing identified mineral phases. The white arrows images indicate the existence of olivine in both spherules.

In the case of plagioclase, most single-crystal clasts are coarse-grained (> 50 μm), showing a few large diffraction spots or streaks (e.g., A-14, Fig. 3a). Some clasts are polycrystalline (fine-grained) (> 5 μm), homogeneous Debye rings (e.g., A-26, Fig 3c). Clasts having intermediate grain size (15–50 μm) (e.g., B-47, Fig 3b) show rings of individual spots.

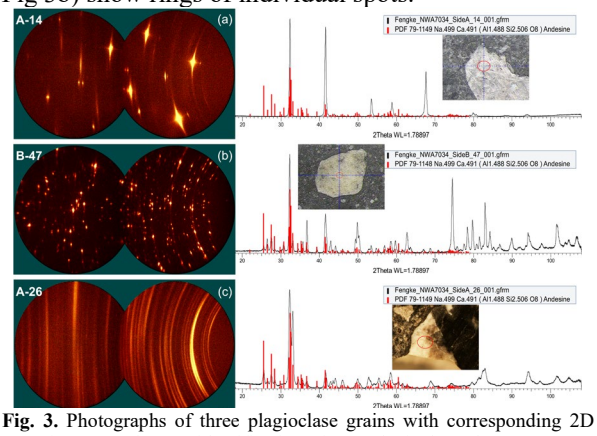

Fig. 3. Photographs of three plagioclase grains with corresponding 2D XRD images and X-ray identification of pure plagioclase phase.

Shock effects: Most coarse-grained single-crystal clasts in NWA 7034 observed by *in situ* μXRD have shown streaking – presumably due to strain-related mosaicity associated with shock events [10-14,19]. Fig. 4 gives some examples of different shock characteristics. 31 plagioclase clasts have been analyzed using micro-XRD so far, and their average FWHMχ per grain ranges from 0.62° to 6.59°. The maximum average FWHMχ value among enstatite clasts is ~ 8.52°. The most streaked diopside grain (Fig. 4b) FWHMχ value of 8.32°.

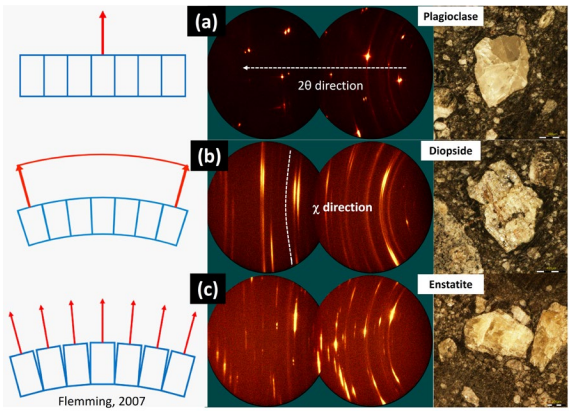

Fig. 4. Photographs of three coarse-grained clasts and corresponding 2D XRD images showing an unstrained single-crystal (a), non-uniformly strained single crystal or "streak" (b), and a series of systematically reoriented mosaic blocks or "asterism" (c).

Discussion: Plagioclase clasts have different grain sizes from fine-grained (< 5 μm) to coarse-grained (> 50 μm), which may be useful to infer their formation environments. Plagioclase has experienced different crystallization rates. The fine-grained plagioclase has cooled rapidly, while intermediate-sized plagioclase grains (15–50 μm) may have been recrystallized. The maximum shock pressure among these plagioclase targets is estimated to be ~22.4 GPa (FWHMχ = 6.59°) based on calibration work on experimentally shocked andesine samples [20]. The estimated maximum shock pressure of enstatite determined by μXRD is estimated to be > 30 GPa based on shock stage assessment work in enstatite chondrites [12].

Conclusions and Future Work: Shock-related mosaicity for single crystal clasts has been studied through measuring FWHMχ of peak intensity along χ to yield quantitative estimates of deformation for plagioclase and pyroxene. In the future, SEM-EDS and EPMA will be done to acquire chemical data of pyroxene, and EBSD will be performed to check the microstructural deformation features on some highly-shocked grains.

References: [1] Agee C.B. et al. (2013) *Science, 339,* 780–785. [2] Schmidt M. E. et al. (2013) *Mineral. Mag., 77,* 2158. [3] Cannon K. M. et al. (2015) *Icarus, 252,*150–153.[4] Tanaka K.L. and Hartmann W.K. (2012) *Elsevier,* 275–298. [5] Baker L. et al. (2005) *Springer,* 3–24. [6] Moser D. E. et al. (2019) *Nature, 12,* 522–527. [7] Stöffler D. and Grieve R. A. F. (1996) *Symposium,* 27, 1996. [8] Stöffler D. (2018) *Meteorit. Planet. Sci.,* 53, 5–49. [9] Wittmann A. et al. (2015) *Meteorit. Planet. Sci.,* 50, 326–352. [10] Li Y. et al. (2019) *GSA*, 51, 333895. [11] Rupert et al. (2020) *Meteorit. Planet. Sci.,* 55, 2224-2240. [12] Izawa M. R. M. et al. (2011) *Meteorit. Planet. Sci.,* 46, 638–651. [13] Pickersgill A.E. et al. (2015) *Meteorit. Planet. Sci.,* 50, 1851–1862. [14] Jenkins, L. E. et al. (2019) *Meteorit. Planet. Sci.,* 54, 902–918. [15] Vaniman D. T. et al. (2014) *Science,* 343, 6169. [16] Cao F. et al. (2017) *LPSC 48th,* #2827. [17] He B. B. (2009) *Wiley,* 426. [18] Bramble M. S. et al. (2015) *Am. Mineral.,* 100, 1899–1911. [19] Flemming R. L. (2007) *Can. J. Earth Sci, 44,* 1333–1346. [20] Cao F. et al. (2020) *LPSC 51st,* # 2114.